Topology Visualization of the Optical Power Flow through a Novel C-Shaped Nano-Aperture

Liying Sun[1]
Physics Department
Stanford University

Rajesh K. Batra[2]
Optical Platform Division
Intel Corporation

Xiaolei Shi[3]
GE Global Research Center

Lambertus Hesselink[4]
Electrical Engineering Department
Stanford University

ABSTRACT

We recently discovered that C-shaped sub-wavelength (nano) metallic apertures when irradiated at specific resonance frequencies have extraordinary power transmission five to six orders of magnitude beyond what is observed for conventional round or square apertures. These apertures produce optical spot sizes as small as 25-50 nm using visible light in the near-field of the aperture with a brightness 10-100 times higher than that of the illuminating beam. A proper understanding into this remarkable phenomenon can aid in the development and understanding of a multitude of applications of these apertures including dense data storage, particle manipulation, and nano-scale photonic devices. Current scalar visualization approaches typically are insufficient to significantly aid in the understanding of these complex near-field optical problems. For example, two common approaches involving either visualization of scalar electromagnetic wave amplitudes in 2-D or rudimentary arrow plots of the vector fields produced in Finite-Difference-Time-Domain simulations are clearly inadequate. Both techniques provide only partial insight into the problem, as only specific planes can be visualized and therefore the global structure of the fields cannot be readily inferred. Understanding of the three-dimensional electromagnetic vector fields and energy flows related to the illumination of nano-sized apertures is critically important in near-field applications, as simple scalar analysis is not suitable at these small dimensions [8].

An ideal visualization tool that has not been used before in studying the optical behavior of near-field apertures is three-dimensional vector field topology. The global view of the vector field structure is deduced by locating singularities (critical points) within the field and augmenting these points with nearby streamlines. We have used for the first time, to the best of our knowledge, three-dimensional topology to analyze the topological differences between a resonant C-shaped nano-aperture and various non-resonant conventional apertures. The topological differences between these apertures are related to the superiority in power throughput of the C-aperture versus conventional round and square sub-wavelength apertures. We demonstrate how topological visualization techniques provide significant insight into the energy enhancement mechanism of the C aperture, and also shed light on critical issues related to the interaction between multiple apertures located in close proximity to each other, which gives rise to cross-talk, for example as a function of distance. Topological techniques allow us to develop design rules for the geometry of these apertures and their desired spot sizes and brightness. The performance of various sub-wavelength apertures can also be compared quantitatively based on their topology. Since topological methods are generically applicable to tensor and vector fields, our approach can be readily extended to provide insight into the broader category of Finite-Difference-Time-Domain nano-photonics and nano-science problems.

CR Categories and Subject Descriptors: I.3.8 [Computer Graphics]: Application; I.4.7 [Image Processing and Computer Vision]: Feature Measurement - Feature representation;I.2 [Applications]: Physical Sciences and Engineering - Engineering.

Additional Keywords: energy flow topology, Finite-Difference-Time-Domain (fdtd), C-aperture, vector field visualization

1 INTRODUCTION

This study describes the application of flow topology visualization techniques to the investigation of extraordinary optical transmission through a novel C-shaped metal nano-aperture. This feature based vector field visualization technique can be extended generally to the flourishing field of Finite-Difference-Time-Domain (FDTD) methods [19] used in many nano-photonics problems [5][11][14][20]. Because of the diverse applications of the FDTD method and the vast amount of information it produces, an effective high-level abstraction of the data set can not only provide critical insight into the physical phenomena, it will also help direct ongoing research efforts.

2 BACKGROUND

The objective of our optics research is to understand the underlying physical mechanism responsible for enormous power throughput for our C-shaped apertures. These specially designed C-apertures, when irradiated at specific resonance frequencies, can have extraordinary power transmission of five to six orders of magnitude greater than that measured for conventional square and round apertures in real metals, and three orders of magnitude greater in ideally conducting metals [15]. We speculate that this extraordinary enhancement in transmission is due to a

{[1]lysun, [3]xiaolei}@stanford.edu
{[2]raj, [4]bert}@kaos.stanford.edu

IEEE Visualization 2004
October 10-15, Austin, Texas, USA
0-7803-8788-0/04/$20.00 ©2004 IEEE

combination of a propagation mode enabled by the C-shaped boundary condition, and the surface plasmon resonance effect [16]. A detailed understanding will help us utilize and optimize these apertures in a great variety of nano-technology applications.

The computation technique we use to study these sub-wavelength apertures is the Finite-Difference-Time-Domain (FDTD) method. In recent years, the FDTD method has become increasingly popular in many scientific and engineering research areas. As a direct solution method for Maxwell's curl equations,

$$\frac{\partial \vec{H}}{\partial t} = -\frac{1}{\mu}\nabla \times \vec{E}; \text{ (Equation 1)}$$

$$\frac{\partial \vec{E}}{\partial t} = -\frac{1}{\varepsilon}\nabla \times \vec{H}; \text{ (Equation 2)}$$

it simulates the continuous electromagnetic waves by sampled numerical data analogs propagating in a computer data space. Solving complex electromagnetic wave interaction problems may require the solution of considerably more than 10^8 field-vector unknowns. At this level of complexity, it is possible to develop detailed, three-dimensional models of complete engineering systems. As FDTD can simulate large structures with much detail, the visualization of the simulation results has become increasingly crucial in understanding information produced by the simulation.

Traditionally, multi-colour maps of the scalar quantities such as field intensity, amplitude and phase angle are used. Cross-sections of the structure are mapped to reveal the 3-D features. Researchers can only combine these 2-dimensional images in their mind's eye in an attempt to grasp the 3-dimensional vectorial reality. Even though some attempts have been made to produce the vector field plots of the fields and power flows, due to the extraordinarily large size of the data set and dense sampling, the results are often more confusing than providing insight. With the development of FDTD simulations in more and more areas of research, effective visualization techniques have become a crucial step toward utilizing the power of this method.

In this study, we apply the vector flow topology techniques we have developed earlier [6][7] to our investigation of the extraordinary optical transmission through the C-shaped nano-apertures. Since this is essentially a near-field phenomenon, and the behaviour of electromagnetic waves in the near field is very different from that of the far field, our knowledge and intuition about the far field often works against our understanding of the physical near-field reality studied here. It is particularly important that visualization of the simulated data provides accurate and elucidating insight into the physics and nature of the interactions in the region of interest. The vector flow topology technique proves to be effective in that it finds critical points in the data set, and provides a skeleton of the three-dimensional flow, thus simplifying the data set for visualization without compromising the critical information embedded in the flow structure. The technique also enables comparisons of topological structures between fields. With the help of such three-dimensional representations of the power flow field both at resonance and off-resonance, we are able to see in detail how the power throughput are affected by the coupling between the front and back surfaces, and the mechanism of power collection and transmission of such apertures. In addition, these pictures have helped researchers to bridge the gap between the data and the physics, and build intuition for further studies.

3 Description of Simulation

3.1 Simulation Space

The simulation space is a three-dimensional Cartesian grid lattice bisected by a Perfect Electric Conductor (PEC) plane. The electric ($\vec{E}$) and magnetic ($\vec{H}$) field vector components are located on the lattice according to the arrangement of the cubic Yee cell [19]. The whole simulation space is bound by absorbing boundary layers (PMLs) to imitate infinite space outside. The aperture is located at the centre of the PEC plane. The resolution of the simulation is 5nm. The simulation space size is 130x130x100. The simulation is time stepped until a steady state in the structure has been reached. After some post processing, the steady-state values of the phase and amplitude for each E and H field component, as well as the components of the time-averaged Poynting vectors (Optical Power Flow Vectors)

$$\vec{S} = \frac{1}{2}\vec{E} \times \vec{H}^{*} \text{ (Equation 3)}$$

are obtained for each point in the 3-dimensional lattice that describes the simulation space.

3.2 Numerical Experiments

For illustration purposes, a series of simulations are performed on the following configurations in order to determine the cause of the large performance differences between them.

Group I:

a) A 50 nm x 50 nm square aperture.
b) A 50 nm x 150 nm rectangular aperture.
c) A 150 nm x 50 nm rectangular aperture.

Group II:

a) A short-armed C aperture, not optimum for resonance.
b) The original C aperture, optimised for resonance.
c) A long-armed C aperture, not optimum for resonance.

In each case, the aperture is located on a single layer PEC plane. The input is an electromagnetic plane wave with a wavelength of 500 nm propagating in the +z direction. The E-field of the input wave is polarized in the y-direction. The input wavelength is chosen to be the resonance wavelength of the original C aperture. See the schematics of the simulated structures in Figure (1) and Figure (2).

It has been shown that the transmission has strong polarization dependence. The enhanced transmission occurs when the E field of the input wave is aligned with the arms of the C aperture. A study of Group I apertures will help us understand the polarization dependence. Group II consists of the original C and two variations of it. Studies of these apertures show that the transmission efficiency can be tuned by adjusting the arm length of the C shape.

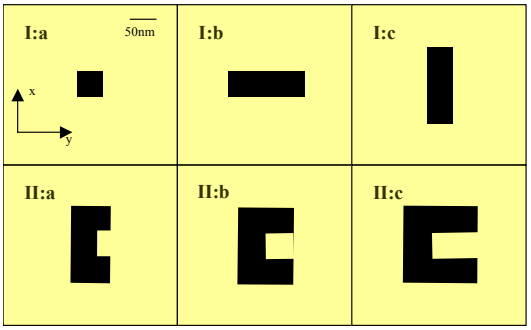

Figure 1 Apertures simulated for transmission comparisons and topology comparisons

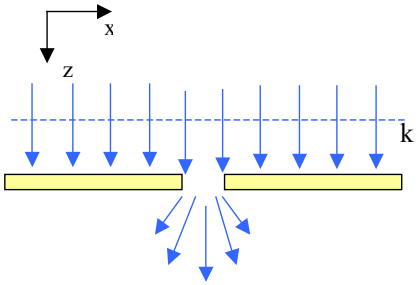

Figure 2 Schematic of single layer PEC containing an aperture

4 Visualization of Data

4.1 Conventional visualization of data

For illustration, color-maps of E field intensities for a C aperture and a square aperture at 50 nm away from the aperture, as well as cross-sections of vector arrow plots of the power flux are presented in Figure (3) and Figure (4).

The field intensity distribution color maps show the extraordinary three or more orders of magnitude field enhancement of the C aperture as compared to a square aperture (magnitudes are normalized to the incident E field intensity).

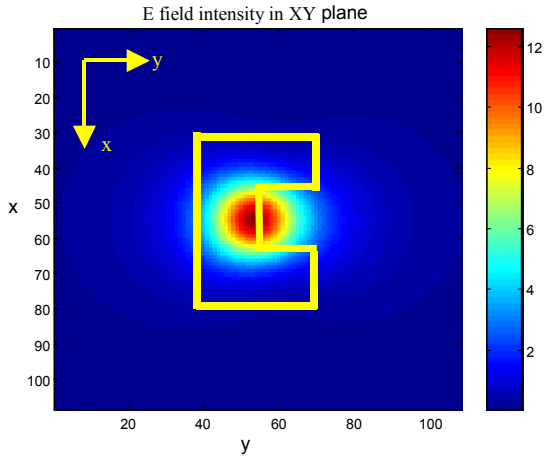

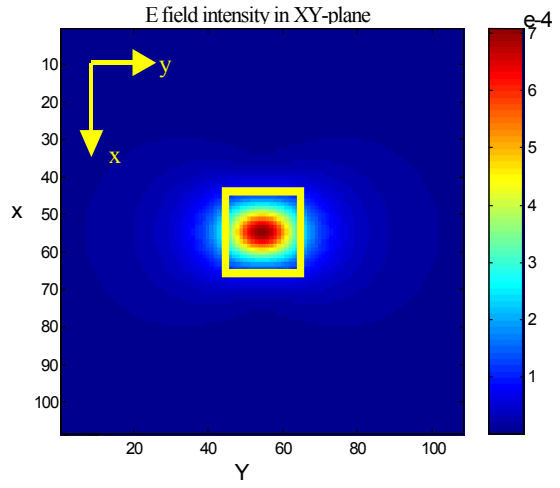

Figure 3 Comparison of the electric field intensity distribution of a C aperture and a 50 nm square aperture

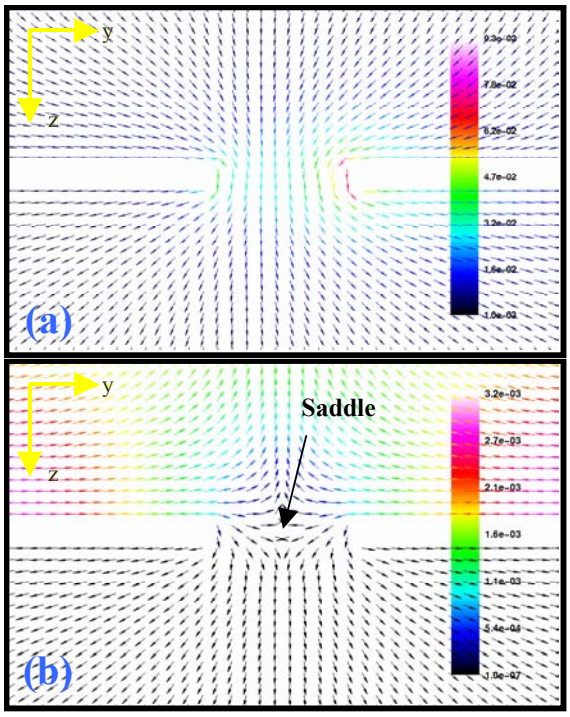

Figure 4 Vector plots of power flux in the YZ-planes cutting through the centers of (a): a C-aperture and (b): a 50 nm square aperture. Color maps the magnitudes of the power flux.

The cross-section of the vector plots shows that the geometry of the C shape effectively collects power from its surroundings, and it is able to funnel that power through the aperture continuously. For the square aperture case, the aperture does not have a propagation mode at this wavelength, most of the power incident on the aperture is reflected, forming a saddle point very close to the aperture.

These two-dimensional plots provide some insight into the characteristics of the C aperture power transmission enhancement, and the effect thereon of the aperture boundary conditions.

However, because of limited data views, it is still very hard to surmise the global behavior of the spatial evolution of the power flow.

4.2 Flow Topology Approach

4.2.1 Theory

Topology is a branch of geometry, dealing with properties that persist under continuous transformations. Topology is a natural framework for the study of many flow problems. Flows can be characterized by particle paths that change as function of position and time. The topology of the flow field consisting of critical points and their connections provides a simple, yet complete representation of the steady state particle paths [10][18].

Essential to the study of flow topology are the integral paths (phase portraits) formed by the solution of a set of differential equations. Poincarè discovered that the behavior of this space could be characterized by critical (singular) points where the vector field is identically zero. Under continuous transformations, critical points remain invariant and are fundamental topological properties. The behavior of the flow about a critical point can be analyzed by investigating the integral paths (streamlines) in the neighborhood of the critical point. Initially, we constrain the analysis to two-dimensions. For points sufficiently close to the critical point (a distance dx, dy away) in most cases a first order Taylor series expansion of the vector field is sufficient as described by Equation 4.

$$u_i \approx \frac{\partial u_i}{\partial x_j} dx_j \quad \text{(Equation 4)}$$

where u is the velocity vector, and x is the position vector. If the system has linearly independent eigenvectors, the basis for the space of solutions is the vector-valued functions:

$$x_j(t) = v_j e^{\lambda_j t} \quad \text{(Equation 5)}$$

where λ_j is the eigenvalue associated with v_j. For complex eigenvalues without multiplicity, the solution can be expressed in terms of sines and cosines. Therefore, one can derive all the possible trajectories near a critical point. The flow pattern is completely determined by the Jacobian matrix:

$$J_{ij} = \frac{\partial u_i}{\partial x_j} \quad \text{(Equation 6)}$$

It can be shown that a particle that originates at a non-critical point will never reach a critical point in finite time and critical points are the only points in the vector field where tangent curves may touch each other. In the case of steady state, tangent curves represent streamlines.

Based on these observations, the power of topological visualization can be understood. Given the critical points and their principal tangent curves, an observer can visually infer the shape of other tangent curves and hence the structure of the whole vector field. This feature based data representation is a high-level description that avoids visual clutter and provides information in a more compact, clear and meaningful way.

We can take another step forward, by representing the basic flow patterns in a manner that allows us to define a quantitative measure of closeness between fields. This technique will prove useful when comparing various apertures. The characteristic equation for the matrix of Equation 6 is:

$$\lambda^2 - P\lambda + Q = 0 \quad \text{(Equation 7)}$$

where P = trace(J) and Q = det(J). If P and Q form the dimensions of a space, all simple critical points can be mapped into this space. This forms the well known P-Q stability diagram[3][12]. Assuming that like patterns are considered closer to one another, the parabolic nature of the P-Q space does not easily lend itself to comparing two critical points. If instead, a new space is defined based on the discriminant of the characteristic equation as follows:

$$\alpha' = P$$
$$\beta' = \text{sgn}(P^2 - 4Q)\sqrt{|P^2 - 4Q|} \quad \text{(Equation 8)}$$

It can be proven that the ratio of $\frac{\beta'}{\alpha'}$ determines the local topological structure of a simple critical point. Therefore, a further simplification can be made by normalizing α' and β' as follows:

$$\alpha = \frac{\alpha'}{\sqrt{\alpha'^2 + \beta'^2}}, \beta = \frac{\beta'}{\sqrt{\alpha'^2 + \beta'^2}} \quad \text{(Equation 9)}$$

The local topological structure of a simple critical point can be characterized by the angle:

$$\theta = \tan^{-1}\left(\frac{\beta}{\alpha}\right) \quad \text{(Equation 10)}$$

Figure 5 represents the simple critical points in $\alpha - \beta$ space.

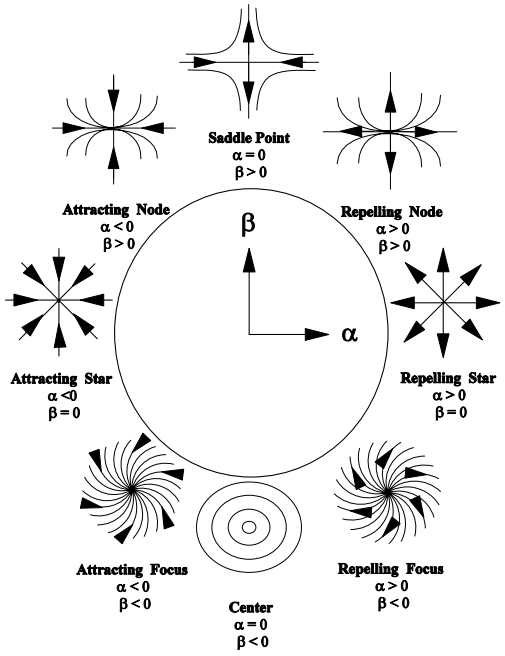

Figure 5: Simple critical points mapped into alpha, beta space.

The change in pattern is seen as a continuous transformation.

Non-hyperbolic critical points are denoted as points (0°, 45°, 135°, 180°, and 270°) and illuminate bifurcations[9]. To compare two critical points, one can measure the difference between their angles.

As our analysis is in three dimensional space, we must analyze Equation 4 for i,j = 1,2,3. The characteristic equation becomes:

$$\lambda^3 + P\lambda^2 + Q\lambda + R = 0 \quad \text{(Equation 11)}$$

where $P = -trace(J)$, $Q = \frac{1}{2}\left(P^2 - trace(J^2)\right)$, and $R = -\det(J)$. Three distinct eigenvalues are possible, along with three eigenvectors. The flow field can be decomposed into fundamental solution trajectories along its eigenvector planes as demonstrated by Reyn[13] and Chong et al.[4]. All other solution trajectories converge (or diverge) to these eigenvector planes. Therefore a critical point in 3-D can be defined by a set of three (α, β) values. Each (α, β) point corresponds to a solution trajectory formed in the respective eigenvector plane. In reference [1][2], the seven possible classes along with their respective phase portraits are illustrated. In this paper, we simply will describe the critical points by either their (α, β) values or the corresponding mnemonic: DRN: Degenerate, Repelling Node, RS: Repelling Star, RN: Repelling Node, RF: Repelling Focus, C: Center, AF: Attracting Focus, AS: Attracting Star, AN: Attracting Node, DAN: Degenerate Attracting Node, and S: Saddle.

4.2.2 Group I Data Visualization

As a start, the topologies of the first three numerical experiments in Group I are shown in Figure 6. The critical points for each aperture are identified and marked according to their (α, β) values. The arrowed lines are the computed tangent lines originating from the critical points; red lines are the outgoing tangent lines, and the yellow ones are incoming tangent lines. Several important features of nano-aperture transmission can be derived directly from the topologies.

In this sets of simulations, the topologies of the power flow fields are rather similar. Each topology has five critical points; a pair of (S, S, AN)s in the x-direction, a pair of (RF)s in the y-direction (i.e. the polarization direction of the input electromagnetic field), and a single (S, S, AN) at the center. We can identify the center (S, S, AN) in Figure (6-I:a) to be the 'saddle' that appears in Figure (4-b).

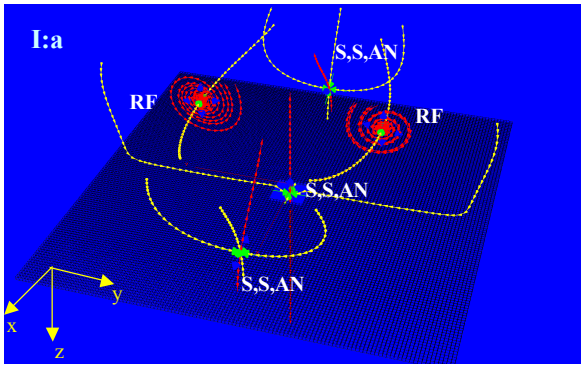

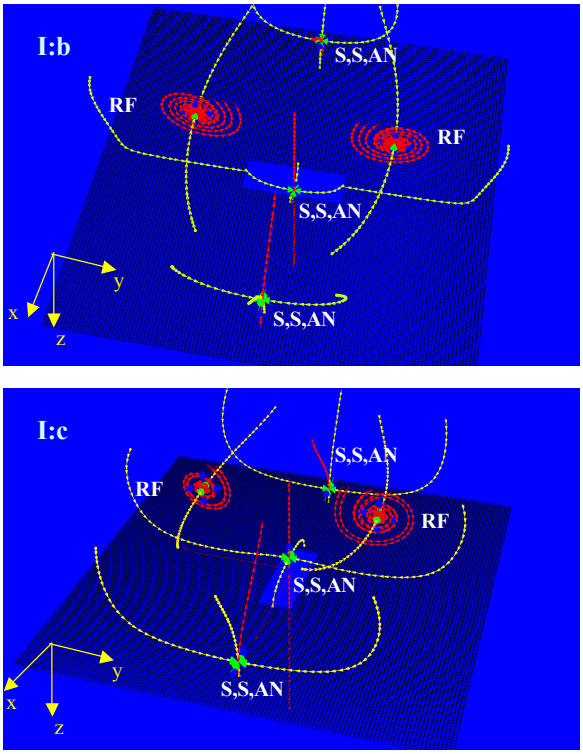

Figure 6 Topologies of power flow in structures of Group I

Firstly, the distribution of critical points has a distinct dependence on the incident light polarization. For the square aperture, the geometry is symmetric in the x and y directions. However, the critical points along the x- direction are totally different from those along the y- direction. In the x-direction, there is a pair of (S, S, AN) critical points; in the y-direction, there is a pair of (RF) critical points. This broken symmetry is induced by the incident light polarization, which is in the y-direction.

Secondly, the z-position of the central critical point (S,S,AN) can be adjusted by changing the aperture geometry. When elongating the square aperture I:a in the y direction to I:b, the z-position drops below the aperture plane. When elongating I:a in the x-direction, the z-position goes above the aperture plane. The z-position of this critical point has direct impact on power transmission since it is a saddle point in both the xz and yz plane. Physically, a higher z-position should allow more power transmission through the aperture. This is consistent with our FDTD power transmission efficiency calculation, as shown in detail in Table 1. The values of transmission are all normalized to the value in the square case.

Table 1. Comparison of transmission and z-location of center (S, S, AN)s of Group I cases

	Square	50nm x 150nm rectangle	150nm x 50nm rectangle
Normalized transmission	1.00	0.89	220.75
Relative z-position	0.00	-32.5 nm	37.5 nm

Lastly, the x, y positions of the other four critical points are

similar in the three cases, and they roughly define a region of 1λ x 1λ, which is approximately the 'region of influence' of the apertures. Physically, these four critical points are speculated to be related to surface waves around the aperture, which is consistent with their separation distance ~λ. In the current simulation, the simulation space is limited to ~1.3λx1.3λ. We expect to see more similar critical points when the simulation space is further extended. The transmission performance of small apertures is strongly influenced by both the aperture transmission mode and surface plasmons waves [16]. Since there is no transmission mode involved in the Group I apertures, these four critical points should be associated with the surface waves. As the interaction of the surface waves with aperture transmission and other nano-structures is not well understood, the 3D topological analysis provides a unique and powerful tool to gain helpful insights.

4.2.3 Group II Data Visualization

The topologies of the Group II cases show a more complex structure due to the effect of the protruding PEC metal piece that makes a rectangular aperture into a C-shaped aperture. Figure 7 shows the short (II:a)and long (II:c) armed off-resonance C-aperture cases. Figure 8 shows the resonant C-aperture (II:b) case (resonant apertures have higher power throughput). For the II:a and II:c cases, the same set of 5 critical points from the Group I cases remain, and are located at similar positions as before. At the tips of the protruding PEC metal piece, there are four more critical points, a pair of (AF)s attached to the top surface, and a pair of (RF)s attached to the bottom surface. These new points are considered to be associated with the C-aperture waveguide mode and act as direct coupling agents between the front and back surfaces of the aperture.

The differences between the II:a and II:c cases can be clearly noticed from the relative distributions of the two RF critical points along the y-direction and the central critical point (S,S,AN). In the II:a case, the two RF points are located far above the central (S,S,AN) point and the central saddle point pushes all the tangent lines from the two (RF) points away from the aperture. In the II:c case, the central (S,S,AN) point is noticeably moved upward closer to the two (RF) points and in effect, some of the tangent lines from the two (RF) points are pushed downward through the aperture. This indicates that more transmission should be expected in the II:c aperture than in the II:a case. This is actually confirmed by comparison of the transmission efficiencies of these apertures, as shown in Table 2. (The values are normalized to the I:a square case value.) Clearly, the relative position between the central saddle point and the two RF points has a strong impact on the aperture transmission performance.

For the resonant C-aperture II:b, its critical points can be similarly divided into two groups: 5 critical points above the aperture surface, and 4 critical points attached to the tip of the protruding metal piece. The 4 "around the tip" critical points are similar to those of the off-resonant C-apertures II:a and II:c. Their theta values (Equation 10) are almost identical. However, the critical points above the aperture surface show a much different appearance from the off-resonant cases.

The three critical points in the y-z plane have transformed from a (RF) pair and a (S, S, AN) center into a (S, S, RN) (S, S, AN) pair and a (S, S, RN) center. The tangent lines that connect these three critical points form a 'bubble' that is replenished from its sides, and inside which all the power circulates down into the aperture. The (S, S, RN) (S, S, AN) pair is located at much higher locations away from the aperture, compared with the off-resonant cases in Figure 7.

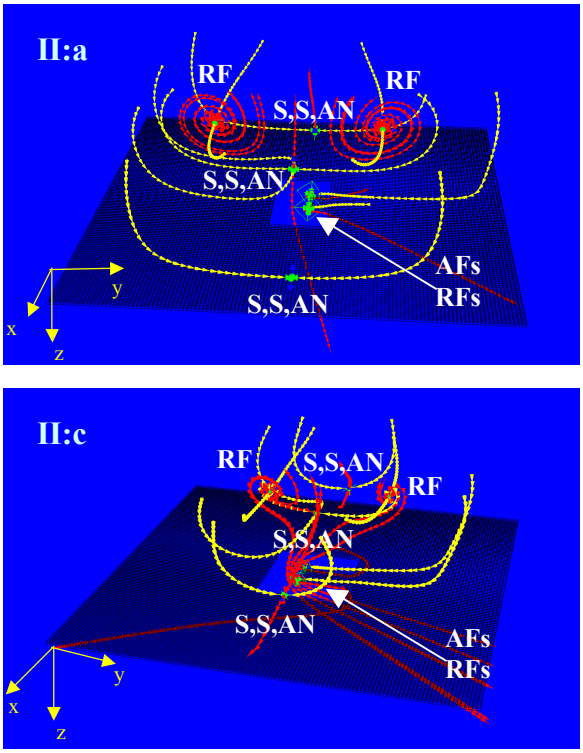

Figure 7 Topology of power flow in II:a and II:c

Table 2. Comparison of transmission in II:a, II:b and II:c cases

	II:a	II:b	II:c
Normalized transmission	654.42	3289.64	932.53

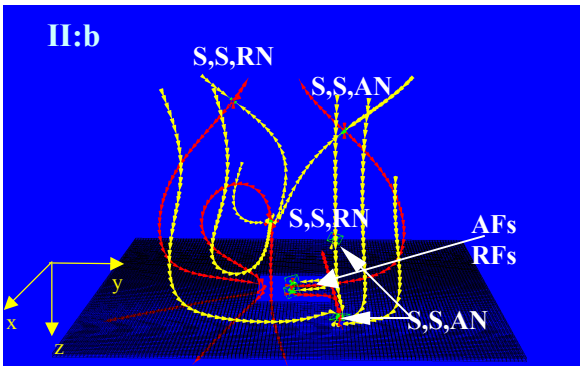

Figure 8 Power flow topology of resonant II:c

The topological change of critical point patterns from off- (Figure 7) to on-resonance cases (Figure 8) is intriguing. When the C-aperture arm length increases monotonically from II:a to II:b to II:c, the transmission passes through a resonant peak in the II:b

condition. The change in the topology of the critical points is commensurate with the occurrence of the resonance phenomenon. However, the detailed process of the change in topology as a function of the arm length increases is not clear and is under investigation. One possible scenario could be: when the C-aperture arm length increases toward the resonance condition, the central saddle point moves steadily upward and pushes the two (RF) points higher up. This provides increased power transmission through the aperture, as the saddle tends to block power flow at a lower position. At resonance, the two (RF)s are forced to be "unwound" to saddle/node points. When the arm length further increases, the central saddle point drops toward the aperture and the saddle/node points are "wound up" again to (RF) points. As more calculation results are available, we expect to get a more complete picture for the resonance pattern changes in relation to shape changes in the aperture.

Since these critical points are thought to be related with surface waves, the topological plots provide strong indication that the resonance in the C-aperture transmission is a surface wave initiated resonance. It is clear that high transmission through the C-aperture is enabled by a propagation waveguide mode, which is also consistent with the strong power flows at the four "around the tip" critical points. Further investigation into the coupling between the surface critical points and the "around the tip" critical points should elucidate the mutual coupling between the surface wave and the waveguide mode.

From the topologies of the Group I and Group II cases, we can infer that the unique three-critical-point combination [a (S, S, RN) (S, S, AN) pair and a (S, S, RN) center] is a clear indicator of resonance. When a structure is irradiated at an off-resonance wavelength, a pair of (RF)s drive the power flow back up, blocking efficient transmission through the hole. However, when the structure is irradiated at its resonance wavelength, the PEC metal tip creates enough pulling action, so that the topology changes into that of the II:b case where the transmission is greatly enhanced.

4.2.4 Future Work

Since we have only included a limited and discrete set of geometries in this paper, simulations of other types of geometries as well as more transitional geometries will be studied to form a more complete picture of the evolution of the flow. Effects of other relevant parameters such as incident wavelength, incident angles will also be considered. In addition, the power flow is created by the more fundamental E and H fields, topological studies on these fields in space as well as on the metal surface will provide more insight in the interaction of surface waves, and aid in aperture optimization and application. A complete characterization of the critical points, which include the physical location, the eigenvalues and eigenvectors will be carried out. Simulations that are of several wavelengths in size, and/or include multiple apertures will also be carried out to study the aperture interactions via propagating optical fields as well as surface plasmon waves.

5 CONCLUSION

In this study, we use the technique of vector flow topology to visualize the power flow around and through a novel C-shaped nano-aperture and its variants. By analyzing the data set using this abstraction method, we are able to gain understanding of the critical factors that affect the power transmission of these apertures. Specifically, the topology analysis shows that: 1) the polarization effect on nano-aperture transmission is clearly shown in the flow topology; 2) the z-position of the central saddle point can be adjusted by aperture geometry and has direct impact on nano-aperture transmission efficiency; 3) the surface wave impact and waveguide mode impact on nano-aperture transmission can be identified from the critical points; 4) the size of the interaction region can be identified by the locations of the critical points; 5) a drastic change of the critical point patterns happens at resonant transmission; 6) the changes in the characteristic critical point topology provides direct evidence that the C-aperture resonance is initiated by surface plasmons. This study shows that vector field topology techniques are very suitable for applications that involve large three-dimensional power flow vector field data sets. This feature-based visualization technique holds great promise in promoting the usefulness and applicability of FDTD simulations in many engineering and basic science branches.

REFERENCES

[1] Rajesh Batra and Yingmei Lavin and Lambertus Hesselink, *Topology Based Comparison Technique for Vector Fields Using Earth Mover's Distance,* Scientific Computing in Chemical Engineering II, Vol. 1, p181-195, (Springer Verlag May 1998), International Workshop at Technical University Hamburg-Harburg at Hamburg, Germany. Invited paper.

[2] Rajesh Batra and Lambertus Hesselink, *Feature Comparisons Of 3-D Vector Fields Using Earth Mover's Distance*, Proc. IEEE Visualization '99, p105-114, (IEEE Computer Society Press, Los Alamitos, CA 1999).

[3] William E. Boyce and Richard C. DiPrima, *Elemetrary Differential Equations and Boundary Value Problems,* 4th. Ed., (John Wiley & Sons, 1986).

[4] M. S. Chong and A. E. Perry and B. J. Cantwell, *A general classification of three-dimensional flow fields*, Physics of Fluids A, Vol 2**,** No. 5, p765-777, (1990).

[5] Hagness et al. *J. Lightwave Technology*, pp. 2154-2165, (1997)

[6] J. Helman; L. Hesselink, *Representation And Display of Vector Field Topology In Fluid Flow Data Sets*, IEEE Computers; special issue on Visualization and Scientific Data, Vol. 22, p27—36, No. 8, (August 1989).

[7] J. Helman, L..Hesselink, *Visualizing Vector Field Topology in Fluid Flows*, IEEE Computer Graphics and Applications, Vol. 11, No. 3, p36-46. , (May 1991).

[8] John D. Jackson, *Classical Electrodynamics* 3rd Ed. (John Wiley & Sons, Inc), Chapter 10.5. (1998)

[9] Yingmei Lavin, *Topology based methods for vector field comparisons,* Stanford University (2000).

[10] H.K. Moffatt *The Topological (as opposed to the analytical) approach to fluid and plasma flow problems*, Topological Fluid Mechanics, Proceedings of the IUTAM Symposium, (August 1989).

[11] O. Painter et al. , *Science*, pp. 1819-1821, (June 11, 1999).

[12] A.E. Perry and B.D. Fairlie *Critical Points in Flow Patterns*,

Advances in Geophysics B Vol. 18, p299-315, (1974).

[13] John W. Reyn, *Classification and Description of the Singular Points of a System of Three Linear Differential Equations*, Zeitschrift für angewandte Mathematik und Physik (ZAMP), Vol.15, p540-557 (July 1964).

[14] Laurent Salomon et al. *Near-field Distribution of Optical Transmission of Periodic Subwavelength Holes in a Metal Film,* Physical Review Letters, Vol. 86, No. 6, (February 2001)

[15] Xiaolei Shi, Robert Thornton, Lambertus Hesselink, *A Nano-aperture with 1000x Power Throughput Enhancement for Very Small Aperture Laser system (VSAL)*, Proc. of SPIE, Vol. 4342, p320, (2001).

[16] Xiaolei Shi, Lambertus Hesselink, *Design of a C aperture to achieve λ/10 resolution and resonant transmission*, Journal of Optical Society of America, Vol 21 N. 7, p1305 (July 2004).

[17] Xiaolei Shi, *Resonant optical transmission through a single sub-wavelength aperture for near field applications*, Ph.D dissertation, Stanford University, (2003).

[18] Scheuermann, Hamann, joy, Kollmann. Visulizing Local Vector Field Topology. SPIE Journal of Electronic Imaging, Vol 9, No. 4, p356-367, (October, 2000)

[19] A. Taflove, S.C. Hagness, *Computational Electrodynamics the finite-different-time-domain method*, 2nd Ed. (Artech House 2000).

[20] R. Wannemacher, *Plasmon-supported transmission of light through nanometric holes in metallic thin films,* Optics Communications, (August 2001)